Linking Molecular Structure to Thermal and Electronic Properties of Functional Dicationic Salts

Coby J. Clarke,[ab] Patrick J. Morgan,[b] Jason P. Hallett[a] and Peter Licence[b]*

(a) Department of Chemical Engineering, Imperial College London, Imperial College Rd, Kensington, London SW7 2AZ, UK

(b) GSK Carbon Neutral Laboratory, The University of Nottingham, Nottingham, Triumph Rd, Lenton, Nottingham NG7 2GA, UK

**coby.clarke@nottingham.ac.uk*

ABSTRACT. The two major properties that underpin ionic liquids are tunability and the potential to create task-specific media. Together these properties allow ionic liquids to surpass the roles long held by traditional molecular solvents. However, at elevated temperatures, or under prolonged heating, the structural components that impart such properties decompose or degrade. Dicationic pyridine salts present new opportunities to extend functionality and tunability to high temperatures because they are coordinating and thermally robust. In this work, we present three structurally related series of dicationic pyridine salts, which have been characterised by a wide array of techniques to link thermal and electronic properties to structural variation. The phase transitions and thermal stabilities of the salts were significantly influenced by small structural changes, and several new candidates for high temperature based applications were identified. The electron density, and therefore the electron donating ability, of the pyridine functional group could also be controlled by structural variation of cations and anions. Therefore, dicationic pyridine salts are highly tunable choices for task-specific solvents at elevated temperatures. Importantly, thermally robust solvents not only extend operational ranges, but also reduce the need to replace or replenish solvents that degrade over time at temperatures commonly employed in industrial settings (i.e., 150-200 °C); solvent lifetimes are extended, and production is reduced. This is a critical requirement for complex media such as ionic liquids, which have high economic and environmental production costs.

KEYWORDS: Functional Ionic Liquids, Salts, Thermally Stable, Electronic Structure, X-ray photoelectron spectroscopy, Thermogravimetric Analysis, Differential Scanning Calorimetry

Introduction

Ionic liquids are modular and highly tunable liquids composed of discreet anions and cations.[1] Strong electrostatic interactions prevent ionic liquids from evaporating at atmospheric pressure,[2] which effectively eliminates atmospheric emissions — the primary reason for their early adoption as green solvents.[3] Unfortunately, the duality of ionic liquids were quickly realised, and several major concerns were highlighted that imposed uncertainty over the future of ionic liquids as neoteric solvents.[4,5] However, as ionic liquid applications grew and evolved from the lab to commercial technologies, their disadvantages drew focus and ways to mitigate their shortcomings were conceived. Selected, but important, examples have included: (i) replacement of complex aromatic heterocycles for simple amines to reduce cost and environmental footprints for scale-up;[6] (ii) substituting (eco)toxic structures for biocompatible groups to reduce toxicity profiles and improve health and safety;[7] (iii) switching from aprotic ionic liquids to protic equivalents that are easily made by acid-base neutralisation.[8] Many of these strategies were designed to target specific limitations of ionic liquids; however, an incidental consequence of most strategies was the introduction of new molecular bonds susceptible to thermolysis.[9,10] Thus, the latest generation of ionic liquids generally have reduced thermal stabilities that restrict operating temperatures and lead to the build-up of decomposition products that change physicochemical properties, react with reagents, or poison catalysts.

Thermally stable ionic liquids can be prepared,[11] and in recent years efforts have been made to bridge the gap between ionic liquid and molten salts that operate at high temperatures (i.e. >> 400 °C, far beyond the capability of most organic molecules).[12,13] However, increasing the thermal stabilities of ionic liquids always incurs a tunability penalty because most anions (i.e. nucleophilic halides) and functional groups must be eliminated at temperatures above 150-200 °C.[14–17] Notable

examples of thermally stable organic salts are tetraarylphosphonium cations[18] and geminal dicationic ionic liquids.[19] The improved thermal stability of geminal dications over monocations is thought to be due to a cage effect, which allows the decomposition products to reform the original dicationic salt.[11] Most current studies and emerging applications that require thermally stable ionic liquids are centred around geminal dications because they are easily synthesised from commercial reagents. Liu *et al*. found that the rate constants of bimolecular reactions are enhanced in dicationic ionic liquids, which highlighted that two cationic head groups also present other advantages alongside improved thermal stability.[20] Importantly, their investigation was limited by the melting points of the geminal dications, which demonstrated that wide liquid ranges were just as important as thermal stability when designing ionic liquids for specific applications. Melting points of dicationic salts can be suppressed by increasing the length of the alkyl chain spacer.[21] Polyethers linkers can also be used to decrease glass transitions temperatures, but inclusion of functional groups on the dication usually compromises thermal stability.[22] Xylyl-bridged dications can be prepared with both low temperature glass transitions and high thermal stabilities,[23] although the solid to liquid transitions in this class of ionic liquid can be significantly raised by low symmetry inorganic anions,[24] and the xylyl-groups does not include functional heteroatoms. Appending functional groups to organic anions also reduces thermal stabilities for mono- and dications alike.[25] The most common thermally robust anion continues to be the bis(trifluoromethanesulfonyl)imide anion (abbreviated $[NTf_2]^-$) because it is commercially available and inherently thermally robust — primarily because it is weakly interacting.[26]

It is difficult to predict what structures are capable of withstanding extreme temperatures, especially for highly modular molecules such as ionic liquids. Generally, a wide variety of structure have to be prepared and thermally characterised to understand high temperature

chemistry because bond strengths do not necessarily reflect thermal stabilities.[27] For tetraarylphosphonium salts, several key publications have identified some functional groups suitable for applications at elevated temperatures;[12,13] however, they are generally weakly interacting and therefore have limited task-specificity (i.e. ethers). Despite this, some thermally tolerant functional groups can be incorporated into tetraarylphosphonium salt to increase π-π interactions with aromatic molecules, which can significantly improve the performance of high temperature GC columns loaded with tetraarylphosphonium stationary phases.[28] These columns improve the separation and quantification of environmentally hazardous aromatic compounds such as polycyclic aromatic hydrocarbons (PAHs) and polychlorinated biphenyls (PCBs), and the ultra-high thermal stability of the ionic liquid reduces the bleeding of the stationary phase out of the column to improve lifetime. This is a key example that highlights the growing need for thermally robust functional ionic liquids. Unfortunately, aryl- groups do improve thermal stability of phosphonium salts but at the expense of raising the melting point, which ultimately reduces the operating window of the ionic liquid. However, a recent study by Rabideau *et al*. in 2020 showed that the melting points of tetraarylphosphonium salts are inversely correlated to the dipole moment of the cation,[29] which demonstrates that targeted functionalisation can be an effective strategy to lower melting points and expand the liquid ranges of the thermally robust salts.

Recently, we reported a pyridine functional dicationic ionic liquid stable up to ≈ 400 °C that was capable of coordinating a metal catalyst.[30] When combined with $[NTf_2]^-$ anions, the resulting ionic liquid had a glass transition at -54.7 °C, which was 51.7 °C higher than the geminal dication $[C_6(C_1Im)][NTf_2]$, but with the added advantage of a functional group. Hence, the ionic liquid was the first example of a new strategy to extend the tunability and designer aspect of ionic liquids to elevated temperatures. Importantly, thermally robust solvents also have extended lifetimes at

intermediate temperatures (i.e., 150-200 °C), which reduces the need to replace and replenish solvents and lessens the environmental burden of producing highly complex molecules. Such temperatures are also commonly encountered in industrial settings, where prolonged lifetimes make ionic liquids more economically feasible.

In this work, we present a structure based investigation of the thermal and electronic properties of pyridine functionalised dicationic ionic liquids (**Figure 1**), which were inspired by robust CNC-pincer type molecules.[31] We provide a comprehensive understanding of how small structural changes significantly influence thermal transitions and the electron donating abilities of pyridine functional groups, which demonstrates that CNC-pincer type ionic liquids can be versatile solvent media. Furthermore, a common limitation for increasing thermal stabilities of ionic liquids is the simultaneous increase in the melting points or glass transitions, often above the 100 °C mark that has long been used as an upper limit in the definition of ionic liquids. Thermal transitions dictate operational temperature ranges, so in this work we present a graphical representation of liquid ranges, along with recommended parameters, to help identify suitable candidates for applications across all temperature ranges.

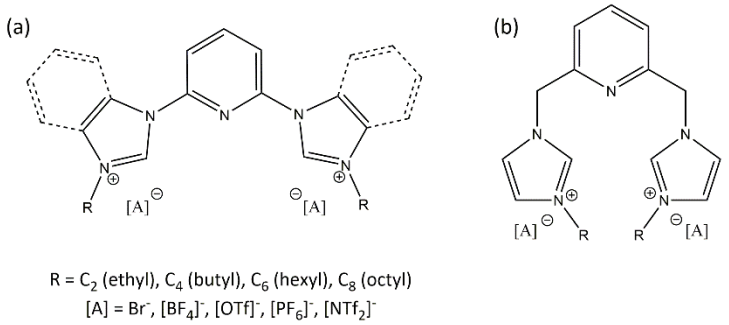

Figure 1. Structures of the CNC-pincer inspired salts based on (a) 2,6-bis(alkylimidazolium)pyridine (abbrev. $[(C_nIm)_2Py][A]_2$, without dashed bonds) and 2,6-

bis(alkylbenzimidazolium)pyridine, (abbrev. $[(C_8BzIm)_2Py][A]_2$, with dashed bonds), and (b) 2,6-bis(alkyimidazoliummethyl)pyridine (abbrev. $[(C_8ImC_1)_2Py][A]_2$).

Experimental

Synthesis and characterisation data for $[(C_nIm)_2Py][A]_2$ and $[(C_8BzIm)_2Py][A]_2$ salts are shown in the supporting information, along with all thermal analysis data, NMR, X-ray photoelectron spectroscopy (XPS), and crystallography data. Synthesis, characterisation, and thermal analysis of $[(C_8ImC_1)_2Py][A]_2$ salts have previously been published,[30] but full XPS analysis is presented in this work and all peak fitted data is shown in the supporting information.

Instruments and Methods

Differential scanning calorimetry (DSC) was recorded on a TA Instruments Discovery DSC2500 with an RCS90 capable of cooling to -90 °C. All samples were prepared in aluminium Tzero hermetic pans with pin hole lids and sealed shut. The DSC was fully calibrated before use, including baseline conditioning, temperature, cell constant, heat capacity, and MDSC calibration with indium and sapphire calibration samples supplied by TA Instruments. A dry nitrogen purge at 50 mL min^{-1} was used for all experiments. A drying step (120 °C for 30 min) was used to drive water from the samples and, unless otherwise stated, all samples were first melted and held isothermally for 1-5 mins to remove thermal history of the sample. Heating rates and modes (i.e., standard or modulated) were varied and unless otherwise stated all transitions (e.g., T_g, T_{cc}, T_{ss}, T_m) were measured from heating cycles at 10 °C min^{-1} and values were taken as peak onset (T_m, T_{cc}, T_{ss}) or the midpoint (T_g) determined by half-height. Modulated DSC (MDSC) was recorded on the same instrument using temperature modulation with amplitudes of 1-2 °C, periods of 40-60 s, and heating rates of 2°C min^{-1} to ensure relevant transitions had sufficient modulation cycles. Data was

analysed in TA Instruments TRIOS software and graphs were plotted as normalised units of W g^{-1}. Enthalpy of fusion (ΔH^{fus}) and entropy of fusion (ΔS^{fus}) values were calculated from separate DSC experiments consisting of 6 cycles at 10 °C min^{-1} and the first cycles were omitted to remove thermal history of the samples. Normalised peak enthalpies (J g^{-1}) of the melting transitions were calculated and averaged, and the standard deviation of the mean was calculated as the error. ΔH^{fus} was calculated from these values in units of kJ mol^{-1}, and ΔS^{fus} was calculated in units of J mol^{-1} K^{-1} from ΔH^{fus} and T_m, which was taken as the onset temperature of the melting peak, according to the equation: $\Delta S_m = \Delta H_m / T_m$, which is valid over a melting transition because the change in free energy is zero.[12]

Thermogravimetric analysis (TGA) was recorded on a TA Instruments Discovery TGA 550 under a dry nitrogen purge of 50 mL min^{-1} and samples were loaded into high temperature platinum pans. Pans were cleaned by heating to 1000 °C for 1 hour in 100 mL min^{-1} air and additionally cleaned by sonicating in 37 % HCl every 3-4 samples. Kinetic analysis was carried out using Modulated TGA (MTGA)[32] which was compared to two samples analysed by the Flynn-Wall isoconversion method[33] (i.e. ASTM E1641). Hi-Res ramping at 2 °C min^{-1} was used with a resolution of 6.00 and sensitivity of 1.00. Activation energies (E_a) were measured at 10 % mass loss to ensure sufficient cycles had passed (SI, **Figure S84**) and to maintain consistency in measurements as E_a varied throughout experiments. Average E_a values and standard deviations were determined from 20 min windows centred around 10% mass loss (SI, **Figure S85-98**). Note: in two cases these windows were shifted to cover steady state data and avoid signal spikes; all plots show the windows and signals used to calculate E_a values. Optimal MTGA parameters were determined using the common IL $[C_2C_1Im][NTf_2]$ which was purchased from Sigma Aldrich and used as received. An E_a value of 127.2 ± 2.1 kJ mol^{-1} was calculated from the chosen parameters

(SI, **Figure S85**), which were a temperature amplitude of 5 °C and a period of 200 s. The E_a for $[C_2C_1Im][NTf_2]$ has previously been determined[34] by an isothermal TGA method to be 131 kJ mol^{-1}, which was only 1.7 kJ mol^{-1} higher than the upper value found by MTGA. Hence, MTGA derived E_a values were consistent with previously reported methods. The two samples analysed by the Flynn-Wall method were $[(C_8Im)_2Py][NTf_2]_2$ (SI, **Figure S99-100**) and $[(C_8BzIm)_2Py][NTf_2]_2$ (SI, **Figure S101-102**) and the E_a values were 166.3 kJ mol^{-1} and 185.7 kJ mol^{-1}, respectively. Both values were marginally higher (by 5.7 kJ mol^{-1} and 12.2 kJ mol^{-1}) than the MTGA derived E_a values of 160.6 kJ mol^{-1} and 173.5 kJ mol^{-1}. Both Flynn-Wall and MTGA methods are model free and both measure how a sample responds to a change in heating rate; however, the MTGA method condenses multiple experiments into a single run by modulating the temperature. Therefore, although MTGA underestimated the E_a values relative to the Flynn-Wall method, values could be compared because of the consistency in their underestimations. Xu *et al*. have recently reviewed ionic liquid thermal stabilities and they provide an overview of the different isoconversional and Arrhenius kinetics analysis methods.[35]

Simultaneous thermal analysis (STA) was recorded on a NETZSCH STA 449F5 with PtRh (80/20) pans under a dry nitrogen purge of 40 mL min^{-1}, and samples were heated at 10 °C min^{-1} to 600 °C. TGA-mass spectrometry (TGA-MS) was measured with a Mettler Toledo TGA/DSC 1LF/UMX with a Hiden Analytical HPR20-QIC evolved gas spectrometer. Samples were loaded into 70 μL Pt pans and heated under a dry nitrogen purge of 50 mL min^{-1} with a ramp rate of 10 °C min^{-1} to 100 °C, held isothermally for 10 min to remove residual water, then ramped at 10 °C min^{-1} to 600 °C. Single crystals of $[(C_8Im)_2Py][OTf]_2$ and $[(C_8BzIm)_2Py][OTf]_2$ were grown by vapour diffusion of diethyl ether into a saturated acetone solution of the salt and analysed by X-ray diffraction on Agilent GV1000 Atlas and SuperNova diffractometers with Cu Kα radiation (λ

= 1.54184). Full crystal data and instrument details are reported in the supporting information (SI, **Table S7**).

Anion chromatography (AC) measurements were undertaken on a Thermofisher ICS5000+ with a Dionex IonPac™ AS20 (2 x 250 mm) analytical column and AG20 (2 x 50 mm) guard column, with a step gradient initially composed of 95 % 18.2 MΩ cm^{-1} water and 5% 100 mM NaOH (to elute Br^-), followed by 20% HPLC grade acetonitrile (99.9%), 75 % water and 5% 100 mM NaOH (to elute other ions). A flow of 0.25 mL min^{-1} was used, with an AERS500e 2 mm electrochemical suppressor (effective eluent strength was 5 mM OH^-), and analytes were detected *via* conductivity at 35 °C.[36,37]

XPS was measured on a Kratos Axis Ultra Spectrometer with a monochromated Al Kα source of 1486.6 eV, a concentric hemispherical analyser (CHA), hybrid magnetic/electrostatic optics, and a multichannel plate and delay line detector (DLD). The incident angle was 30° and the collection angle was 0° to the surface normal. An entrance aperture of 300 by 700 μm^2 was used with a pass energy of 80 eV for wide scans and 20 eV for high resolution scans. Binding energies (E_B) were calibrated to the following photoemissions: the Au $4f_{7/2}$ at 83.96 eV, the Ag $3d_{5/2}$ at 368.21 eV, and the and Cu $2p_{3/2}$ at 932.62 eV. Samples were mounted on to a stainless steel sample bar with double sided sticky tape and degassed overnight to 10^{-7} mbar in a transfer chamber before being moved to the analysis chamber which had a base pressure of 10^{-9} mbar. Samples were charge neutralised during analysis and the measurement error was determined by the manufacturer to be 0.1 eV. All data was converted to VAMAS file format and imported to CasaXPS for analysis. XP spectra were charge corrected by referencing aliphatic signals of octyl (C_8) carbons to 285.0 eV, and shorter chains were referenced to the respective imidazolium N 1s E_B values of the C_8 analogues.[38]

Results and Discussion

The first step in our work was to prepare a range of $[(C_nIm)_2Py][NTf_2]_2$ (where n = 2, 4, 6, and 8) salts to examine how alkyl chain length affected thermal properties. $[NTf_2]^-$ anions were desirable because they have been shown to give low melting temperatures (T_m) and high thermal decomposition temperatures (T_d).[34] A range of different anions with variable basicities (e.g. $[BF_4]^-$, $[OTf]^-$, $[PF_6]^-$) were also selected and the corresponding salts of both $[(C_8Im)_2Py][A]_2$ and $[(C_8BzIm)_2Py][A]_2$ were synthesised to investigate anion and cation structural effects. All products were isolated as white powders so none of the salts prepared in this work were room temperature ionic liquids (RTILs). Ionic liquid purity was confirmed by several techniques, including NMR, HR-MS, elemental analysis, and ion chromatography (IC). NMR showed that all ionic liquids were free from common organic contaminants, while HRMS was used to confirm identity. The purity of hydrophobic ionic liquids were also confirmed by elemental analysis, which was not possible for hygroscopic ionic liquids such as those containing hydrophilic Br^- and $[BF_4]^-$ anions. For ionic liquids with polyatomic anions, IC confirmed that the residual halide content was below 0.006 % (60 ppm), and for the hydrophobic benzimidazolium salts the residual halide content was below the detection limit of the IC (SI, **Table S1**). The most common impurities found in ionic liquid are residual alkylimidazoles, residual halide ions (from ion metathesis reactions), water, and solvents.[39,40] These impurities can significantly affect physical properties such as viscosity;[41] however, thermal parameters are generally less sensitive to residual impurities. For example, Valkenburg *et al.* found that Cl^- ion impurities have negligible effects on T_{onset} values in TGA and negligible effects on T_m values in DSC, whereas water can dramatically affect T_m values but not T_{onset} values.[42] Given that several of the isolated salts were hygroscopic, we chose to employ pre-

drying steps in all thermal analysis experiments (see Experimental Section).[43] Thermal analysis of all salts therefore gave accurate thermal parameters (**Table 1**) that were used to link structure to thermal properties.

Six of the thirteen salts characterised in this work were identified as ionic liquids by DSC because their melting points were below 100 °C. For the $[(C_nIm)_2Py][NTf_2]_2$ series, DSC showed that ethyl chain lengths gave the highest T_m values, which were just above 100 °C. As alkyl chain lengths increased, the T_m values decreased to a minimum at 65.5 °C for octyl chains. Previous measurements have shown that the T_m and T_g values of monocationic ionic liquids generally reach a minimum value for hexyl- and octyl- chain lengths, although this can change depending on the identity of the anion.[44] Longer chains are better at disrupting the coulombic interactions of cations and anions, which helps to suppress their melting points; however, as chains lengths continue to increase, Van der Waals forces between aliphatic chains act to raise the melting points.[44] Similar trends have also been observed for geminal imidazolium dicationic salts,[45] but the identity of both the cation and anion can have drastic effects on this trend.[46,47]

$[(C_nIm)_2Py][NTf_2]_2$ salts readily formed super cooled liquids that underwent glass transitions (T_g), and in some cases (n = 2, 6, and 8) cold crystallization (T_{cc}) occurred, followed by solid-solid transitions (T_{ss}) of the crystallised samples, which finally re-melted. This type of behaviour has previously been observed in some monocationic ionic liquids.[48] The enthalpies of fusion (ΔH^{fus}) values for the $[(C_nIm)_2Py][NTf_2]_2$ series (excluding $n = 4$ which consistently formed a supercooled liquid without crystallizing) decreased by 15.9 kJ mol^{-1} as the alkyl chain length increased from ethyl- to octyl-, while the entropies of fusion (ΔS^{fus}) decreased by 33.5 J mol^{-1} K^{-1}. These

corresponded to a 35.7% decrease in ΔH^{fus} and a 28.2% decrease in ΔS^{fus}, meaning that the T_m decrease was primarily enthalpically driven. Melting peaks for the $[(C_nIm)_2Py][NTf_2]_2$ series displayed peak broadening as the alkyl chain length increased (**Figure 2**). Broadening has been linked to conformational flexibility for dications with benzene linkers, which hinted that the pyridine bridged dications reported in this work could occupy different conformational states.[49] For the $[(C_8Im)_2Py][A]_2$ series, DSC data showed that the lowest T_m was achieved with $[NTf_2]^-$ anions, while $[BF_4]^-$, $[OTf]^-$, and $[PF_6]^-$ anions gave T_m values above 100 °C. Interestingly, the T_m measured for $[(C_8Im)_2Py]Br_2$ was lower than all other salts (except $[(C_8Im)_2Py][NTf_2]_2$) which is a trend rarely observed in monocationic ionic liquids. This observation hinted towards new molecular scale interactions specific to CNC-pincer type salts; molecular interactions and conformations will be discussed later in more detail.

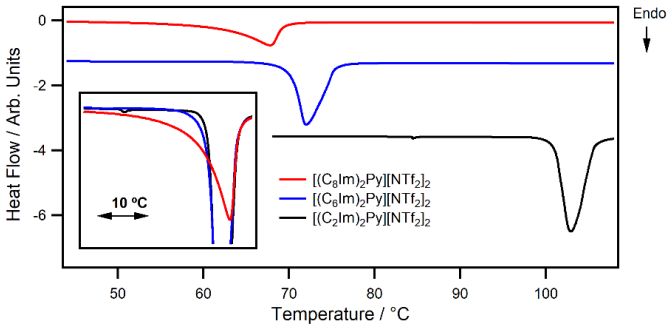

Figure 2. DSC melting peaks at 10 °C min^{-1} for $[(C_nIm)_2Py][NTf_2]_2$ where n = 2 (black), 6 (blue), and 8 (red), with an inset window showing the melting peaks overlaid on the $[(C_8Im)_2Py][NTf_2]_2$ signal.

The phase transitions of benzimidazolium salts varied significantly with anion type. For example, an endothermic decomposition was found to immediately follow melting of $[(C_8BzIm)_2Py]Br_2$ (SI, **Figure S77**); however, amorphous $[(C_8BzIm)_2Py][NTf_2]_2$ melted at 49.8

°C to form a stable supercooled liquid with a T_g 219 °C below the T_m of $[(C_8BzIm)_2Py]Br_2$. Moreover, the effects of anions on T_m did not follow the orders commonly found in monocationic ionic liquids, and links to anion properties such as size and basicity were difficult to conclude for benzimidazolium salts. The low T_m values of the $[NTf_2]^-$ salt relative to the Br^-, $[BF_4]^-$, $[OTf]^-$ and $[PF_6]^-$ analogues suggested that charge diffuse anions with large volume could disrupt the π-π stacking commonly found in benzimidazolium derivatives.[50] In this work, we observed an increase in T_m when Br^- was exchanged for the larger $[PF_6]^-$ anion in both $[(C_8Im)_2Py][A]_2$ and $[(C_8BzIm)_2Py][A]_2$. A decrease in T_m usually occurs when switching Br^- to $[PF_6]^-$ in monocationic imidazolium salts,[51] but an increase in T_m has been reported for one other monocationic benzimidazolium salt[52] (there are limited reports for benzimidazolium thermal properties). The $[PF_6]^-$ anion has an extremely low hydrogen bond acceptor (HBA) ability compared to most other anions,[53] which indicated that H-bonding was as important as anion size and flexibility for lowering melting points of pyridine bridged salts.

Bulky ions introduce disorder in the solid state, which is why ionic liquid with anions such as $[NTf_2]^-$ or $[FAP]^-$ usually have low ΔS^{fus} values.[16] Generally, the ΔS^{fus} values of benzimidazolium salts were lower than imidazolium analogues. Unlike aliphatic chains, the aromatic ring of benzimidazole is ridged, and therefore does not lead to increased degrees of freedom in the liquid phase but should lead to improved packing in the solid state due to π-π stacking. The decrease in ΔS^{fus} was thus either due to lower degrees of flexibility in the liquid state, or improved packing in the solid state. For $[(C_8BzIm)_2Py][OTf]_2$ relative to the imidazolium analogue $[(C_8Im)_2Py][OTf]_2$, a decrease in ΔH^{fus} of 6.8% was measured and a decrease in ΔS^{fus} of 18.6% was measured.

Therefore, substituting imidazolium for benzimidazolium groups produced an entropically driven increase in T_m.

After finding that solid-to-liquid phase change behaviour was highly dependent on anion and cation structure, we wanted to see how thermal stability was affected by small structural changes and whether dicationic pyridine salts were viable candidates for applications at elevated temperatures. For the $[(C_nIm)_2Py][NTf_2]_2$ series, TGA data showed that increasing the alkyl chain length marginally decrease the temperature at which 1% mass loss occurred ($T_{1\%}$) by 18 °C (**Table 1**; SI, **Figure S66**). This was reflected in the relatively consisted E_a of T_d values which were ≈ 160 kJ mol^{-1}. Typically, thermal stabilities of monocationic ionic liquids decrease with increasing alkyl chain length, but the difference in T_{onset} is usually less than 30 °C.[34] Similar decreases in T_{onset} have also been observed for geminal dicationic ionic liquids with longer bridging chains.[30] This decrease has previously been attributed to the increased disruption of electrostatic interactions between anions and cations by long alkyl chains, and to the improved stability of carbocation and radical decomposition products for long chains.[34,35] In this work, nucleophilic anions significantly reduce the thermal stability of both $[(C_8Im)_2Py][A]_2$ and $[(C_8BzIm)_2Py][A]_2$ salts *via* retro-S_N2 T_d (SI, **Figure S67-68**), which was supported by sharp endothermic signals observed in STA data (SI, **Figure S70**). The E_a of T_d for Br^- salts were ≈ 131 kJ mol^{-1}, which was marginally higher than those of monocationic halide salts.[34] Nucleophilic anions such as halides are known to cause the largest reductions in thermal stabilities for all ionic liquid families.[34]

The highest $T_{1\%}$ value was obtained for $[(C_8BzIm)_2Py][NTf_2]_2$ and was 28 °C higher than that of the imidazolium analogue $[(C_8Im)_2Py][NTf_2]_2$, which corresponded to a 12.9 kJ mol^{-1} increase in E_a. This suggested that replacing imidazolium groups for benzimidazolium groups was a feasible

option for improving thermal stability. However, the increase in thermal stability was small when compared to the $T_{1\%}$ value previously obtained for the extremely thermally robust methylpyridine-bridged analogue $[(C_8ImC_1)_2Py][NTf_2]$ ($T_{1\%}$ = 395.6 °C).[30] Despite this, many of the salts reported in this work had very high thermal stabilities when compared to monocationic salts with functional groups such as amines,[17] carboxylic acids,[54] and nitriles.[55] The highest E_a of T_d values were obtained for $[OTf]^-$ salts which were ≈ 25-30 kJ mol^{-1} higher than $[BF_4]^-$ and $[PF_6]^-$ analogues for both $[(C_8Im)_2Py][A]_2$ and $[(C_8BzIm)_2Py][A]_2$ cations. $[BF_4]^-$ and $[PF_6]^-$ anions are known to thermally decompose to release HF,[56] which could potentially react with pyridine functional groups to compromise thermal stability. The E_a values reported in this work are higher than most thermally stable monocationic ILs,[34] which was expected because of the improved thermal stability of dicationic ILs relative to monocationic counterparts.[57]

Table 1. Thermal properties (°C) of $[(C_nIm)_2Py][A]$ and $[(C_8BzIm)_2Py][A]$ salts acquired from DSC and MDSC (T_m, T_g, T_{cc}, T_{ss}, ΔH^{fus}, ΔS^{fus}), STA ($T_{m\ (amorph.)}$, endo/exo), TGA (T_{onset}, $T_{1\%}$), and MTGA (E_a) measurements under nitrogen atmosphere.

Cation	Anion	T_m	T_g	T_{cc}	T_{ss}	T_m (amorph.)	ΔH^{fus} / KJ mol^{-1}	ΔS^{fus} / J mol^{-1} K^{-1}	T_{onset}	$T_{1\%}$	exo/ endo	Liquid Range[f]	E_a / kJ mol^{-1}
$[(C_8Im)_2Py]^{2+}$	$2Br^-$	84.2							265	251	endo	167	131.3 ± 0.95
$[(C_2Im)_2Py]^{2+}$	$2[NTf_2]^-$	101.9	-27.9	5.9	40.8	100.8	44.5 ± 3.5	118.9 ± 9.5	407	363	endo	261	163.4 ± 1.5
$[(C_4Im)_2Py]^{2+}$	$2[NTf_2]^-$	70.0[a]	-26.4[a]			69.2			407	367	endo[e]	393 (297)[g]	160.4 ± 1.2
$[(C_6Im)_2Py]^{2+}$	$2[NTf_2]^-$	70.2	-28.9	5.0	23.9	72.2	39.4 ± 0.18	114.7 ± 0.52	399	361	endo	291	162.0 ± 0.97
$[(C_8Im)_2Py]^{2+}$	$2[NTf_2]^-$	64.7	-27.2	-1.5	20.7	65.3	28.6 ± 0.19	85.4 ± 0.58	379	345	unknown[e]	280	160.6 ± 1.7
$[(C_8Im)_2Py]^{2+}$	$2[BF_4]^-$	104.0				102.1			324	296	endo	192	142.9 ± 1.5
$[(C_8Im)_2Py]^{2+}$	$2[PF_6]^-$	122.3	25.5	76.2	-8.5[b]	121.8			307	238	endo[e]	116	145.3 ± 0.97

$[(C_8Im)_2Py]^{2+}$	$2[OTf]^-$	114.5	6.7	54.0		113.4	38.3 ± 2.6	98.8 ± 6.7	363	247	exo[e]	132	170.1 ± 2.4
$[(C_8BzIm)_2Py]^{2+}$	$2Br^-$	207.5[c]			17.5 133.3	244.0[c]			243	213	endo	6	131.1 ± 0.75
$[(C_8BzIm)_2Py]^{2+}$	$2[NTf_2]^-$		-11.6			49.8			414	373	endo	385 (304)[g]	173.5 ± 1.1
$[(C_8BzIm)_2Py]^{2+}$	$2[BF_4]^-$	220.2			135.0	226.6	33.7 ± 0.61	68.5 ± 1.2	361	309	endo	89	145.2 ± 2.5
$[(C_8BzIm)_2Py]^{2+}$	$2[OTF]^-$	237.1			122.9	237.3	40.9 ± 0.92	80.4 ± 1.7	352	328	endo[e]	91	176.1 ± 1.5
$[(C_8BzIm)_2Py]^{2+}$	$2[PF_6]^-$	239.2[d]	-8.0	198.3[d]	45.5	233.3	34.1 ± 1.6	67.7 ± 3.1	387	312	endo	74	144.0 ± 1.3
$[(C_8ImC1)_2Py]^{2+}$	$2[NTf_2]^-$		-54.7[h]						434[h]	396[h]	endo	451	192.7[h]

(a) Separate cycles; T_g from 10 °C min^{-1} cooling, T_m from quench cooling at 30 °C min^{-1}.

(b) 2 °C min^{-1} heating rate

(c) Simultaneously melts and decomposes

(d) From MDSC at 2 °C min^{-1}

(e) Weak signal

(f) From T_g or T_m to $T_{1\%}$

(g) From $T_{m\ (amorph.)}$ to $T_{1\%}$

(h) From reference 30

TGA-MS and STA data was acquired to gain a mechanistic understanding of thermal decomposition at high temperature to enable the design of thermally robust salts in future studies (**Figure 3**). From STA data, all salts decomposed endothermically except for $[(C_8Im)_2Py][OTf]_2$; however, the weak signals observed in $[(C_4Im)_2Py][NTf_2]_2$, $[(C_8Im)_2Py][OTf]_2$, and $[(C_8Im)_2Py][NTf_2]_2$ STA data made assignment difficult. Nevertheless, weak STA signals indicated that multiple decomposition mechanisms were occurring in parallel,[30] which highlighted the importance of understanding decomposition processes. The weak STA signal of $[(C_8Im)_2Py][NTf_2]_2$ was in contrast to that of $[(C_8BzIm)_2Py][NTf_2]_2$, which showed a clear endothermic decomposition and thus indicated that benzimidazolium groups were influencing the decomposition mechanism. TGA-MS showed that $[(C_8Im)_2Py][NTf_2]_2$ released CO_2 (m/z 44) before signals associated with alkyl-chains loss (m/z 41 and 55) or anion degradation (m/z 64). This observation suggested that $[(C_8Im)_2Py][NTf_2]_2$ initially decomposed by nucleophilic attack of the pyridine functional group on the $[NTf_2]^-$ anion, which acted as an oxygen source. However, $[(C_8BzIm)_2Py][NTf_2]_2$ simultaneously produced signals for CO_2 and alkyl chains, which suggested that the benzimidazolium salt decomposed by alkyl-chain loss (e.g., Hoffman elimination), and this was consistent with an endothermic decomposition. TGA-MS data of the $[OTf]^-$ imidazolium and benzimidazolium analogues also supported that these trends were consistent for each family of cations (SI, **Figure S82-83**) and not unique for $[NTf_2]^-$ salts.

Interestingly, air was found to decrease the $T_{1\%}$ value of $[(C_8Im)_2Py][NTf_2]_2$ and $[(C_8BzIm)_2Py][NTf_2]_2$ by 20 °C and 46 °C, respectively (SI, **Figure S69**). For the benzimidazolium salt, the large decrease in the presence of an oxidising atmosphere suggested that a change in mechanism had occurred, while the smaller decrease for $[(C_8Im)_2Py][NTf_2]_2$ supported that

oxidative decomposition was occurring in both atmospheres. The methylpyridine-bridged $[(C_8ImC_1)_2Py][NTf_2]_2$ salt also underwent a similar decomposition mechanism to that of $[(C_8Im)_2Py][NTf_2]_2$, albeit at a 50 °C higher temperature.[30] This implied that the dication was the limiting factor in terms of stability, and that the pyridine-imidazolium C-N bond was susceptible to thermolysis because of the electron withdrawing effect of the imidazolium groups.

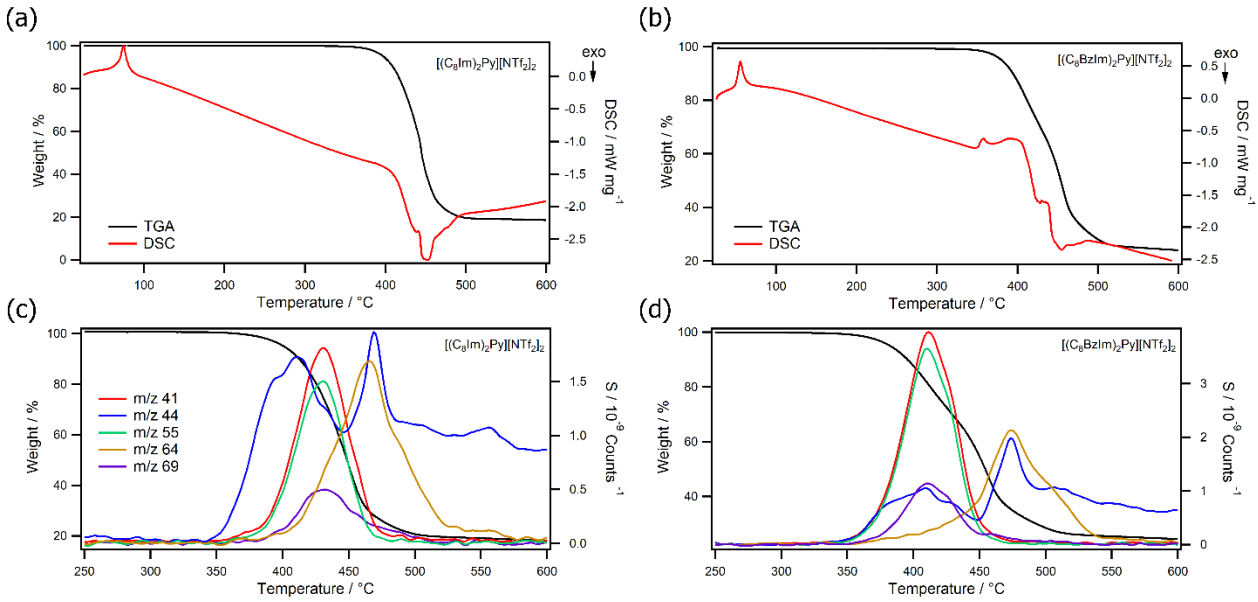

Figure 3. STA (top) and TGA-MS (bottom) data for (a, c) $[(C_8Im)_2Py][NTf_2]_2$ and (b, d) $[(C_8BzIm)_2Py][NTf_2]_2$ at 10 °C min^{-1} under an inert N_2 atmosphere.

Concurrent changes in thermal stabilities and melting points impact the liquid ranges of salts. Since operating ranges are dictated by liquid ranges, a convenient way to visualise and compare the properties of potential new solvents is required. In this work, liquid ranges were calculated for all salts by subtracting either the T_g or T_m (the highest solid-liquid transition was chosen) value from the corresponding $T_{1\%}$ values (which are a conservative estimate of T_d when compared to other parameters such as T_{onset}). The data was also displayed graphically (**Figure 4**), along with selected high temperature organic solvents where the upper values are boiling points as opposed

to T_d. The $[(C_nIm)_2Py][NTf_2]_2$ series had wide ranges for all chain lengths when compared to those of $[(C_8Im)_2Py][A]_2$ with Br^-, $[BF_4]^-$, $[OTf]^-$, and $[PF_6]^-$ anions. The supercooling behaviour of $[(C_4Im)_2Py][NTf_2]_2$ significantly increased the liquid range by 96 °C (i.e., T_g to $T_{1\%}$) compared to that obtained from the $T_{m\ (amorph.)}$ value. This was highlighted on the liquid range plot to show that the temperatures were obtainable, but crystallisation could occur under certain conditions. Considering the T_g value, $[(C_4Im)_2Py][NTf_2]_2$ had the widest liquid range out of all salts presented in this work. However, the value was still 105 °C lower than that previously obtained for $[(C_8ImC_1)_2Py][NTf_2]_2$, which highlighted how addition of a CH_2 linker could significantly improve thermal properties. Similarly, the liquid range of $[(C_8BzIm)_2Py][NTf_2]_2$ was 304 °C from $T_{m\ (amorph.)}$, but 385 °C from the T_g of the supercooled liquid. For $[(C_8BzIm)_2Py][PF_6]_2$, the liquid range was severely compromised by cold crystallisation of the supercooled liquid, but the $[BF_4]^-$ and $[OTf]^-$ analogues had small liquid ranges because of their high melting points. The liquid ranges of high boiling solvents highlighted that the salts presented in this work were more suited for high temperature processes, but the cost of accessing these temperatures were higher T_g/T_m values that effectively shifted the liquid ranges rather than extending them.

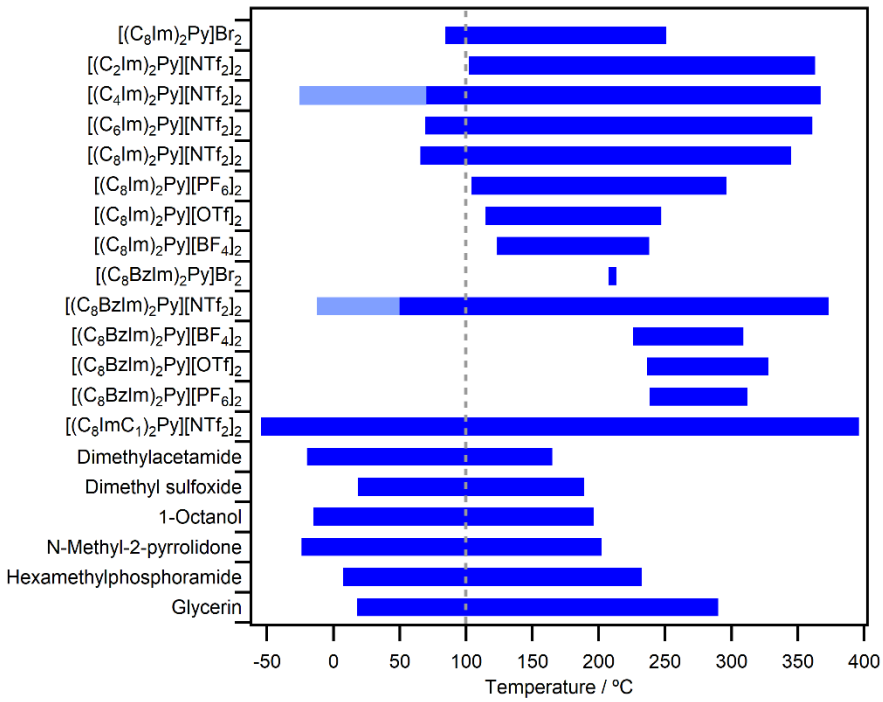

Figure 4. Liquid ranges (dark blue box) from T_m or T_g to $T_{1\%}$ for salts presented in this work with extended scales for supercooled liquids (purple boxes) with high boiling organic solvents for comparison (T_m to boiling point).

Thermal analysis hinted towards the existence of different conformational states in either the solid or liquid states of dicationic pyridine salts. The C-N bonds that link the imidazolium and benzimidazolium group to the 2,6-positions of the pyridine ring can rotate to give different conformations with the C^2 protons pointing inwards towards the CNC cavity, outwards, or a combination of the two (SI, **Figure S104**). Therefore, 2D NOESY was acquired for $[(C_8Im)_2Py][NTf_2]_2$ and $[(C_8BzIm)_2Py][NTf_2]_2$ in DMSO to confirm this possibility. Cross-correlation peaks were observed that supported the presence of both orientations (SI, **Figure S103**) in solution for imidazolium and benzimidazolium analogues. Variable temperature ^{1}H NMR was subsequently used to investigate differences in conformational flexibilities between the analogous salts (SI, **Figure S105-112**). Large chemical shifts during variable temperature ^{1}H NMR

experiments of dicationic imidazolium ionic liquids have previously been attributed to significant changes in the spatial arrangements of cations due to the presence of multiple conformers.[49] In this work, plots of the $\Delta\delta$ for the C^2 protons of $[(C_8Im)_2Py][NTf_2]_2$ and $[(C_8BzIm)_2Py][NTf_2]_2$ against temperature (SI, **Table S5-6**) gave linear plots with gradients of -16.6 x 10^{-4} and -16.8 x 10^{-4}, respectively. Methylbenzene-bridged dicationic salts also analysed by variable temperature ^1H NMR by D'anna *et al.* gave gradients of only -9.3 x 10^{-4}.[49] This suggested that the salts presented in this work were conformationally restricted at low temperatures, but freely rotated at higher temperatures, which resulted in large $\Delta\delta$ shifts.

To complement solution based measurements and gain an insight into molecular conformations, X-ray crystallography was used to characterise $[(C_8Im)_2Py][OTf]_2$, $[(C_8Im)_2Py][NTf_2]_2$ and $[(C_8BzIm)_2Py][OTf]_2$ (**Figure 5**; SI, **Figure S113-118**) — the only salts that formed single crystals in this work. For $[(C_8Im)_2Py][OTf]_2$, the two C^2 carbons of the imidazolium groups were orientated towards the CNC cavity to give a planar structure. Parameters indicative of C^2-H$\cdots O_{(Triflate)}$ hydrogen bonding (SI, **Figure S114a**) were obtained from one triflate anion to two C^2-protons of a single cation; the $[OTf]^-$ anion was located within the CNC cavity. The same planar structure and imidazolium orientations were observed in the $[(C_8Im)_2Py][NTf_2]_2$ analogue, with H-bonding between one $[NTf_2]^-$ anion and four C^2 protons of two dications (SI, **Figure S113**). The larger size of the $[NTf_2]^-$ anion resulted in staggered spatial packing in a single direction, as opposed to the alternated packing observed in the $[OTf]^-$ analogue (SI, **Figure S116b**). For $[(C_8BzIm)_2Py][OTf]_2$, hydrogen bonding from one C^2 proton and one benzene proton to the $[OTf]^-$ anion was observed, which caused the benzimidazolium groups to twist out of plane and to orientate in different directions — one C^2 carbon pointed towards the CNC cavity and the other was flipped outwards. Unlike similar benzimidazolium compounds, limited π-π stacking was observed in the crystal

structure of $[(C_8BzIm)_2Py][OTf]_2$ because of the twisted orientation of the benzimidazolium groups. These observation could explain why strong HBA anions gave lower T_m values compared to weak HBA anions. Furthermore, the large solid-solid transitions observed in DSC (SI, **Figure S59-63**) and STA (SI, **Figure S79-81**) data for $[(C_8BzIm)_2Py][BF_4]_2$, $[(C_8BzIm)_2Py][OTf]_2$, and $[(C_8BzIm)_2Py][PF_6]_2$ may be linked to the rotation of the benzimidazolium groups at higher temperatures. For $[(C_8BzIm)_2Py][OTf]_2$, the solid-solid transition disappeared after the amorphous sample was heated and cooled, but for $[(C_8BzIm)_2Py][BF_4]_2$ the transition remained. Precipitation of the samples from solution undoubtedly gave mixtures of conformational isomers (supported by the NMR data) but heating and cooling of the samples in DSC showed that the orientation was anion-specific and most likely linked to anion size and HBA ability.

Previous work has showed that hydroxyl-functionalised cations have higher thermal stabilities when combined with hydrogen bonding anions.[34] Usually, hydrogen bonding anions are strongly interacting and compromise thermal stability. For our functional dications, hydrogen bonding could theoretically occur between the C^2 proton of one imidazolium ring and the pyridine nitrogen of a different cation, but we do not see any evidence of this in the crystal structures. However, our previous work has highlighted that the pyridine nitrogen in CNC-pincer type ionic liquids is capable of coordinating Lewis acidic metals,[30] so hydrogen bonding cannot be eliminated as an important factor for CNC-pincer salt physicochemical properties.

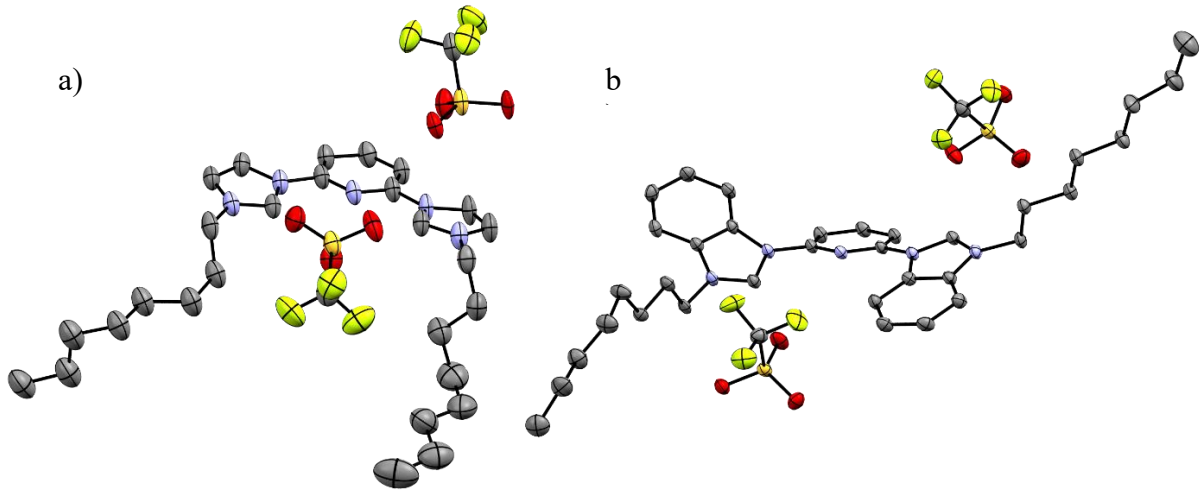

Figure 5. Molecular structure of (a) $[(C_8Im)_2Py][OTf]_2$ and (b) $[(C_8BzIm)_2Py][OTf]_2$. Thermal ellipsoids for the anisotropic displacement parameters represent 50% probability. Alkyl chain disorder and hydrogens have been removed for clarity.

Charge Transfer and Electron Distribution

Following thermal analysis, we aimed to understand the effects of cation structure and anion variation on the electronic properties of the central pyridine functional groups, which are capable of coordinating metal ions for catalytic applications.[30] XPS is a powerful tool for analysing the chemical states of all elements in a sample (except hydrogen) in a single experiment.[58] Hence, we chose to analyse the $[(C_nIm)_2Py][A]_2$ series of salts, which were compared to the analogous $[(C_8ImC_1)_2Py][A]_2$ series and one benzimidazolium salt for a comprehensive understanding of electron distribution about the functional ILs. Firstly, the $[(C_nIm)_2Py][NTf_2]_2$ series of salts showed very little difference in the photoemission binding energies (**SI, Table S8**), with the exception of

the $C^{aliphatic}$ component which moved to higher binding energy as the chain length decreased. This trend has been previously observed for monocationic ionic liquids with low basicity anions such as $[NTf_2]^-$.[59] Substitution of imidazolium groups for benzimidazolium groups did not alter the binding energies of the cations or anions, and the only difference in the photoemission spectra was the addition of the aromatic signals in the C 1s spectrum (SI, **Figure S134**).

Anion variation had a significant effect on the charge distribution of $[(C_8Im)_2Py][A]_2$ salts. For example, switching the basic Br^- anion for the weakly interacting $[NTf_2]^-$ anion caused a 0.5 eV shift to higher binding energy for the imidazolium nitrogen atoms (**Figure 6**c). A similar 0.5 eV shift also occurred for the pyridinium nitrogen atom, which indicated that charge transfer from the anion to the cation could be used to control the electron density around pyridine. The $[(C_8Im)_2Py]^{2+}$ cation is conjugated across the cationic imidazolium groups and the pyridine moiety; however, the methyl-bridged analogue $[(C_8ImC_1)_2Py]^{2+}$ is not. This was reflected in the N 1s imidazolium and pyridine photoemissions of $[(C_8ImC_1)_2Py][A]_2$ salts, which showed 0.3 eV and 0.1 eV shifts, respectively, on changing Cl^- anions for $[NTf_2]^-$ anions. Therefore, the electron density of the pyridine nitrogen of $[(C_8ImC_1)_2Py]^{2+}$ was effectively independent of the choice of anion, but the imidazolium groups were not. The N 1s binding energies of the $[(C_8Im)_2Py][NTf_2]_2$ and $[(C_8ImC_1)_2Py][NTf_2]_2$ pyridine nitrogens were 400.2 eV and 399.5 eV, respectively (**Figure 6**b). This 0.7 eV difference was very large and, in combination with anion variation, suggested that a broad range of electron densities were accessible. This observation highlighted that the structures of functional dicationic ILs were not just intimately linked to thermal properties, but also to the electronic properties of the functional groups.

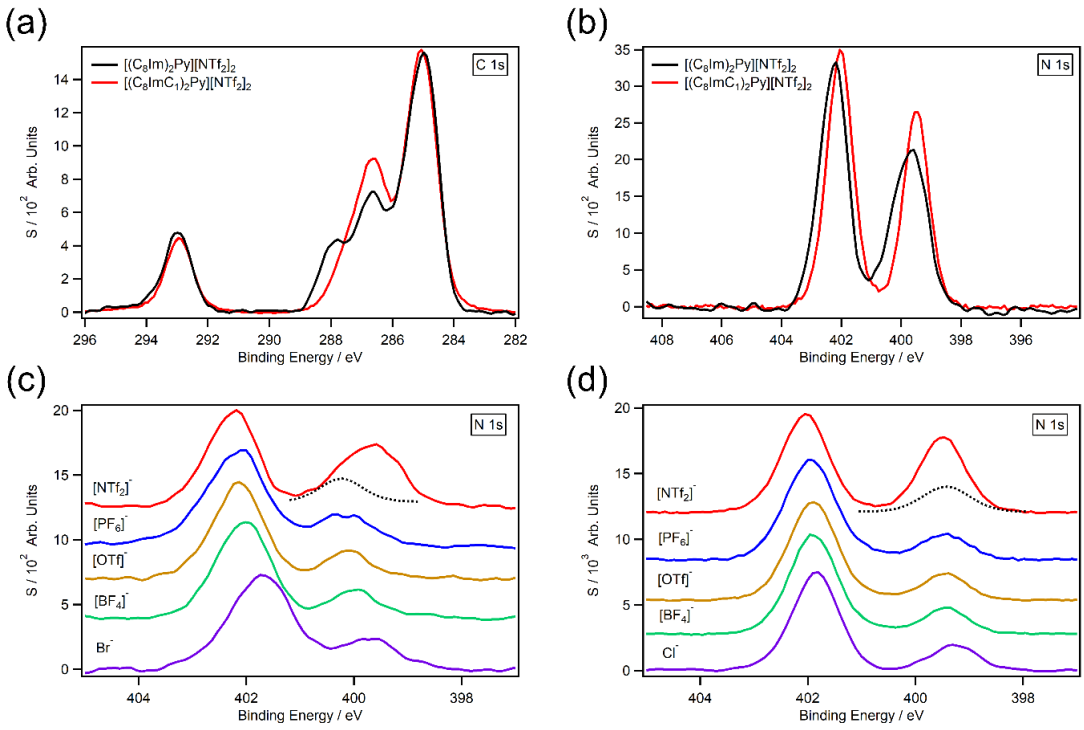

Figure 6. (a-b) Comparison of XPS (a) C 1s and (b) N 1s photoemission spectra for $[(C_8Im)_2Py][NTf_2]_2$ (black) and $[(C_8ImC_1)_2Py][NTf_2]_2$ (red). (c-d) N 1s photoemission spectra for (c) $[(C_8Im)_2Py][A]_2$ and (d) $[(C_8ImC_1)_2Py][A]_2$ with pyridinium N 1s components (dashed line) for the $[NTf_2]^-$ salts.

Conclusions

Three structurally related series of dicationic pyridine salts were prepared with different alkyl chains lengths and anions. The salts were thermally characterised by a wide range of standard and specialised techniques to understand their thermal properties. Many of the salts had high thermal stabilities compared to functional monocationic ionic liquids, but a concurrent increase in melting points or glass transitions was observed in most cases. Thermal data hinted towards the presence of different conformational state in dicationic pyridine salts, which were supported by solution based NMR measurements and solid state based X-ray crystallography. Hydrogen bonding

between cations and anions was identified as an important factor for molecular conformations, and this was linked to the observed thermal properties of the salts. For example, substituting imidazolium groups for benzimidazolium groups led to a decrease in melting points for $[OTf]^-$ and $[NTf_2]^-$ salts due to the twisted conformations of the benzimidazoliums, which prevented π-π stacking. A liquid range plot derived from $T_{1\%}$ and T_m or T_g values was found to be a useful graphical representation to summarise the complex thermal parameters and could find future use as a helpful guide when selecting ionic liquids for an application (particularly at high temperatures).

Electron distribution around the central pyridine moiety was highly dependent on whether a CH_2 linker was present. If imidazolium groups were directly attached to pyridine, the pyridine nitrogen electron density could be controlled by altering the basicity of the anion. This trend did not occur when a CH_2 linker was present, and the central pyridine nitrogen had a far higher electron density because of the absence of conjugation around the aromatic system. By altering both the cation and the anion, a wide range of electron densities could be accessed, which showed that dicationic pyridine salts were highly tunable. Altering anions can dramatically reduce thermal stabilities, but despite this the presence or absence of a CH_2 linker can still be used to control the electron density of the pyridine nitrogen, without severely compromising thermal stability at elevated temperatures.

Dicationic pyridine salts can extend the tunability and task-specific nature of ionic liquids to high temperatures, and the gained stabilities can help prolong solvent lifetimes. This structural variation study has helped to understand the link between structure and properties, but not all samples reported herein are suitable for high temperature applications. The ability to alter the electron density about the functional group is a very powerful strategy to tune task-specific functions for applications such as catalysis. Ionic liquids are often promoted for having wide liquid

ranges, but these are rarely discussed or reported in the literature. A simple way to visualise solvent operating windows is useful for identifying compatible ionic liquids for applications, which is particularly important for studies such as this where a large variety of properties are reported.

ASSOCIATED CONTENT

Supporting Information. Synthesis and characterization, full thermal characterization data, XPS peak fitted high resolution scans, and crystal structure information. The following files are available free of charge, PDF.

AUTHOR INFORMATION

Corresponding Author

*coby.clarke@nottingham.ac.uk

Author Contributions

All data was acquired, analyzed and interpreted by CJC, except for crystallography data which was processed by PJM. The manuscript was written by CJC and PJM and corrected by all authors. All authors have given approval to the final version of the manuscript.

Funding Sources

P.L. thanks EPSRC (EP/K005138/1, EP/P013341/1) and BBSRC (BB/L013940/1) for support. J.P.H. also thanks EPSRC (EP/K038648/1) for support.

ACKNOWLEDGMENT

PJM would like to thank Dr Stephen Argent for helpful advice while processing crystal structures. CJC would like to thank Dr Emily Smith for help acquiring and interpreting XPS data, and Dr Lisa Haigh for acquiring TGA-MS data.

ABBREVIATIONS

DSC, differential scanning calorimetry; MDSC, modulated DSC; TGA, thermogravimetric analysis; MTGA, modulated TGA; STA, simultaneous thermal analysis; TGA-MS, thermogravimetric analysis – mass spectrometry; CHA, concentric hemispherical analyzer; DLD, delay line detector; RTIL, room temperature ionic liquids; NOESY, nuclear Overhauser effect spectroscopy; XPS, X-ray photoelectron spectroscopy.

REFERENCES

(1) Wasserscheid, P.; Welton, T. *Ionic Liquids in Synthesis: Second Edition*; Wiley-VCH, 2008; Vol. 1. https://doi.org/10.1002/9783527621194.

(2) Armstrong, J. P.; Hurst, C.; Jones, R. G.; Licence, P.; Lovelock, K. R. J.; Satterley, C. J.; Villar-Garcia, I. J. Vapourisation of Ionic Liquids. *Phys. Chem. Chem. Phys.* **2007**, *9*, 982–990. https://doi.org/10.1039/b615137j.

(3) Hallett, J. P.; Welton, T. Room-Temperature Ionic Liquids: Solvents for Synthesis and Catalysis. 2. *Chem. Rev.* **2011**, *111* (5), 3508–3576. https://doi.org/10.1021/cr1003248.

(4) Jessop, P. G. Searching for Green Solvents. *Green Chem.* **2011**, *13* (6), 1391. https://doi.org/10.1039/c0gc00797h.

(5) Clarke, C. J.; Tu, W. C.; Levers, O.; Bröhl, A.; Hallett, J. P. Green and Sustainable Solvents in Chemical Processes. *Chem. Rev.* **2018**, *118* (2), 747–800. https://doi.org/10.1021/acs.chemrev.7b00571.

(6) Chen, L.; Sharifzadeh, M.; Mac Dowell, N.; Welton, T.; Shah, N.; Hallett, J. P. Inexpensive Ionic Liquids: [HSO4]--Based Solvent Production at Bulk Scale. *Green Chem.* **2014**, *16* (6), 3098–3106. https://doi.org/10.1039/c4gc00016a.

(7) Billeci, F.; D'anna, F.; Feroci, M.; Cancemi, P.; Feo, S.; Forlino, A.; Tonnelli, F.; Seddon, K. R.; Gunaratne, H. Q. N.; Plechkova, N. V. When Functionalization Becomes Useful: Ionic Liquids with a "Sweet" Appended Moiety Demonstrate Drastically Reduced Toxicological Effects. *ACS Sustain. Chem. Eng.* **2020**, *8* (2), 926–938. https://doi.org/10.1021/acssuschemeng.9b05507.

(8) Greaves, T. L.; Drummond, C. J. Protic Ionic Liquids: Properties and Applications. *Chemical Reviews*. American Chemical Society January 2008, pp 206–237. https://doi.org/10.1021/cr068040u.

(9) Bhattacharyya, S.; Shah, F. U. Thermal Stability of Choline Based Amino Acid Ionic Liquids. *J. Mol. Liq.* **2018**, *266*, 597–602. https://doi.org/10.1016/j.molliq.2018.06.096.

(10) Shmukler, L. E.; Gruzdev, M. S.; Kudryakova, N. O.; Fadeeva, Y. A.; Kolker, A. M.; Safonova, L. P. Thermal Behavior and Electrochemistry of Protic Ionic Liquids Based on Triethylamine with Different Acids. *RSC Adv.* **2016**, *6* (111), 109664–109671. https://doi.org/10.1039/c6ra21360j.

(11) Maton, C.; De Vos, N.; Stevens, C. V. Ionic Liquid Thermal Stabilities: Decomposition

Mechanisms and Analysis Tools. *Chem. Soc. Rev.* **2013**, *42* (13), 5963–5977. https://doi.org/10.1039/c3cs60071h.

(12) Cassity, C. A.; Siu, B.; Soltani, M.; McGeehee, J. L.; Strickland, K. J.; Vo, M.; Salter, E. A.; Stenson, A. C.; Wierzbicki, A.; West, K. N.; et al. The Effect of Structural Modifications on the Thermal Stability, Melting Points and Ion Interactions for a Series of Tetraaryl-Phosphonium-Based Mesothermal Ionic Liquids. *Phys. Chem. Chem. Phys.* **2017**, *19* (47), 31560–31571. https://doi.org/10.1039/c7cp06278h.

(13) Rabideau, B. D.; West, K. N.; Davis, J. H. Making Good on a Promise: Ionic Liquids with Genuinely High Degrees of Thermal Stability. *Chem. Commun.* **2018**, *54* (40), 5019–5031. https://doi.org/10.1039/c8cc01716f.

(14) Xue, Z.; Zhang, Y.; Zhou, X. Q.; Cao, Y.; Mu, T. Thermal Stabilities and Decomposition Mechanism of Amino- and Hydroxyl-Functionalized Ionic Liquids. *Thermochim. Acta* **2014**, *578*, 59–67. https://doi.org/10.1016/j.tca.2013.12.005.

(15) Chambreau, S. D.; Schenk, A. C.; Sheppard, A. J.; Yandek, G. R.; Vaghjiani, G. L.; Maciejewski, J.; Koh, C. J.; Golan, A.; Leone, S. R. Thermal Decomposition Mechanisms of Alkylimidazolium Ionic Liquids with Cyano-Functionalized Anions. *J. Phys. Chem. A* **2014**, *118* (47), 11119–11132. https://doi.org/10.1021/jp5095855.

(16) Zhang, H.; Liu, J.; Li, M.; Yang, B. Functional Groups in Geminal Imidazolium Ionic Compounds and Their Influence on Thermo-Physical Properties. *J. Mol. Liq.* **2018**, *269*, 738–745. https://doi.org/10.1016/j.molliq.2018.08.037.

(17) Liu, S.; Chen, Y.; Shi, Y.; Sun, H.; Zhou, Z.; Mu, T. Investigations on the Thermal Stability

and Decomposition Mechanism of an Amine-Functionalized Ionic Liquid by TGA, NMR, TG-MS Experiments and DFT Calculations. *J. Mol. Liq.* **2015**, *206*, 95–102. https://doi.org/10.1016/j.molliq.2015.02.022.

(18) Soltani, M.; McGeehee, J. L.; Stenson, A. C.; O'Brien, R. A.; Duranty, E. R.; Salter, E. A.; Wierzbicki, A.; Glover, T. G.; Davis, J. H. Ionic Liquids of Superior Thermal Stability. Validation of PPh4+as an Organic Cation of Impressive Thermodynamic Durability. *RSC Adv.* **2020**, *10* (35), 20521–20528. https://doi.org/10.1039/d0ra03220d.

(19) Anderson, J. L.; Ding, R.; Ellern, A.; Armstrong, D. W. Structure and Properties of High Stability Geminal Dicationic Ionic Liquids. *J. Am. Chem. Soc.* **2005**, *127* (2), 593–604. https://doi.org/10.1021/ja046521u.

(20) Liu, K. T. C.; Haines, R. S.; Harper, J. B. The Effect of Bisimidazolium-Based Ionic Liquids on a Bimolecular Substitution Process. Are Two Head(Group)s Better than One? *Org. Biomol. Chem.* **2020**, *18* (37), 7388–7395. https://doi.org/10.1039/d0ob01500h.

(21) Liu, J.; Yang, W.; Li, Z.; Ren, F.; Hao, H. Experimental Investigation of Thermo-Physical Properties of Geminal Dicationic Ionic Compounds for Latent Thermal Energy Storage. *J. Mol. Liq.* **2020**, *307*. https://doi.org/10.1016/j.molliq.2020.112994.

(22) Vélez, J. F.; Vázquez-Santos, M. B.; Amarilla, J. M.; Herradón, B.; Mann, E.; del Río, C.; Morales, E. Geminal Pyrrolidinium and Piperidinium Dicationic Ionic Liquid Electrolytes. Synthesis, Characterization and Cell Performance in LiMn2O4 Rechargeable Lithium Cells. *J. Power Sources* **2019**, *439*, 227098. https://doi.org/10.1016/j.jpowsour.2019.227098.

(23) Boumediene, M.; Haddad, B.; Paolone, A.; Drai, M.; Villemin, D.; Rahmouni, M.; Bresson, S.; Abbas, O. Synthesis, Thermal Stability, Vibrational Spectra and Conformational Studies of Novel Dicationic Meta-Xylyl Linked Bis-1-Methylimidazolium Ionic Liquids. *J. Mol. Struct.* **2019**, *1186*, 68–79. https://doi.org/10.1016/j.molstruc.2019.03.019.

(24) Hadji, D.; Haddad, B.; Brandán, S. A.; Panja, S. K.; Paolone, A.; Drai, M.; Villemin, D.; Bresson, S.; Rahmouni, M. Synthesis, NMR, Raman, Thermal and Nonlinear Optical Properties of Dicationic Ionic Liquids from Experimental and Theoretical Studies. *J. Mol. Struct.* **2020**, *1220*, 128713. https://doi.org/10.1016/j.molstruc.2020.128713.

(25) Vieira, J. C. B.; Paz, A. V; Hennemann, B. L.; Kuhn, B. L.; Bender, C. R.; Meyer, A. R.; Pagliari, A. B.; Villetti, M. A.; Frizzo, C. P. Effect of Large Anions in Thermal Properties and Cation-Anion Interaction Strength of Dicationic Ionic Liquids. *J. Mol. Liq.* **2020**, *298*, 112077. https://doi.org/10.1016/j.molliq.2019.112077.

(26) Benchea, A.; Siu, B.; Soltani, M.; McCants, J. H.; Alan Salter, E.; Wierzbicki, A.; West, K. N.; Davis, J. H. An Evaluation of Anion Suitability for Use in Ionic Liquids with Long-Term, Higherature Thermal Stability. *New J. Chem.* **2017**, *41* (16), 7844–7848. https://doi.org/10.1039/c7nj01788j.

(27) Patil, R. A.; Talebi, M.; Berthod, A.; Armstrong, D. W. Dicationic Ionic Liquid Thermal Decomposition Pathways. *Anal. Bioanal. Chem.* **2018**, *410* (19), 4645–4655. https://doi.org/10.1007/s00216-018-0878-0.

(28) Odugbesi, G. A.; Nan, H.; Soltani, M.; Davis, J. H.; Anderson, J. L. Ultra-High Thermal Stability Perarylated Ionic Liquids as Gas Chromatographic Stationary Phases for the Selective Separation of Polyaromatic Hydrocarbons and Polychlorinated Biphenyls. *J.*

Chromatogr. A **2019**, *1604*, 460466. https://doi.org/10.1016/j.chroma.2019.460466.

(29) Rabideau, B. D.; Soltani, M.; Parker, R. A.; Siu, B.; Salter, E. A.; Wierzbicki, A.; West, K. N.; Davis, J. H. Tuning the Melting Point of Selected Ionic Liquids through Adjustment of the Cation's Dipole Moment. *Phys. Chem. Chem. Phys.* **2020**, *22* (21), 12301–12311. https://doi.org/10.1039/d0cp01214a.

(30) Clarke, C. J.; Bui-Le, L.; Hallett, J. P.; Licence, P. Thermally-Stable Imidazolium Dicationic Ionic Liquids with Pyridine Functional Groups. *ACS Sustain. Chem. Eng.* **2020**, *8* (23), 8762–8772. https://doi.org/10.1021/acssuschemeng.0c02473.

(31) Peris, E.; Loch, J. A.; Mata, J.; Crabtree, R. H. A Pd Complex of a Tridentate Pincer CNC Bis-Carbene Ligand as a Robust Homogenous Heck Catalyst. *Chem. Commun.* **2001**, No. 2, 201–202. https://doi.org/10.1039/b008038l.

(32) Blaine, R. L.; Hahn, B. K. Obtaining Kinetic Parameters by Modulated Thermogravimetry. *J. Therm. Anal. Calorim.* **1998**, *54* (2), 695–704. https://doi.org/10.1023/A:1010171315715.

(33) Mamleev, V.; Bourbigot, S.; Le Bras, M.; Lefebvre, J. *THREE MODEL-FREE METHODS FOR CALCULATION OF ACTIVATION ENERGY IN TG*; 2004; Vol. 78.

(34) Cao, Y.; Mu, T. Comprehensive Investigation on the Thermal Stability of 66 Ionic Liquids by Thermogravimetric Analysis. *Ind. Eng. Chem. Res.* **2014**, *53* (20), 8651–8664. https://doi.org/10.1021/ie5009597.

(35) Xu, C.; Cheng, Z. Thermal Stability of Ionic Liquids: Current Status and Prospects for Future Development. *Processes* **2021**, *9* (2), 337. https://doi.org/10.3390/pr9020337.

(36) Clarke, C. J.; Bui-Le, L.; Corbett, P. J.; Hallett, J. P. Implications for Heavy Metal Extractions from Hyper Saline Brines with [NTf2]-Ionic Liquids: Performance, Solubility, and Cost. *Ind. Eng. Chem. Res.* **2020**, *59* (27), 12536–12544. https://doi.org/10.1021/acs.iecr.9b04722.

(37) Clarke, C. J.; Bui-Le, L.; Hallett, J. Ion Chromatography for Monitoring [NTf 2] − Anion Contaminants in Pure and Saline Water. *Anal. Methods* **2020**, *12* (17), 2244–2252. https://doi.org/10.1039/d0ay00337a.

(38) Villar-Garcia, I. J.; Smith, E. F.; Taylor, A. W.; Qiu, F.; Lovelock, K. R. J.; Jones, R. G.; Licence, P. Charging of Ionic Liquid Surfaces under X-Ray Irradiation: The Measurement of Absolute Binding Energies by XPS. *Phys. Chem. Chem. Phys.* **2011**, *13* (7), 2797–2808. https://doi.org/10.1039/c0cp01587c.

(39) Ab Rani, M. A.; Brant, A.; Crowhurst, L.; Dolan, A.; Lui, M.; Hassan, N. H.; Hallett, J. P.; Hunt, P. A.; Niedermeyer, H.; Perez-Arlandis, J. M.; et al. Understanding the Polarity of Ionic Liquids. *Phys. Chem. Chem. Phys.* **2011**, *13* (37), 16831–16840. https://doi.org/10.1039/c1cp21262a.

(40) Stark, A.; Behrend, P.; Braun, O.; Müller, A.; Ranke, J.; Ondruschka, B.; Jastorff, B. Purity Specification Methods for Ionic Liquids. *Green Chem.* **2008**, *10* (11), 1152–1161. https://doi.org/10.1039/b808532c.

(41) Seddon, K. R.; Stark, A.; Torres, M. J. Influence of Chloride, Water, and Organic Solvents on the Physical Properties of Ionic Liquids. In *Pure and Applied Chemistry*; Walter de Gruyter GmbH, 2000; Vol. 72, pp 2275–2287. https://doi.org/10.1351/pac200072122275.

(42) Valkenburg, M. E. V.; Vaughn, R. L.; Williams, M.; Wilkes, J. S. Thermochemistry of Ionic Liquid Heat-Transfer Fluids. In *Thermochimica Acta*; Elsevier, 2005; Vol. 425, pp 181–188. https://doi.org/10.1016/j.tca.2004.11.013.

(43) Gómez, E.; Calvar, N.; Domínguez, Á. Thermal Behaviour of Pure Ionic Liquids. In *Ionic Liquids - Current State of the Art*; Handy, S. T., Ed.; IntechOpen, 2015. https://doi.org/10.5772/59271.

(44) López-Martin, I.; Burello, E.; Davey, P. N.; Seddon, K. R.; Rothenberg, G. Anion and Cation Effects on Imidazolium Salt Melting Points: A Descriptor Modelling Study. *ChemPhysChem* **2007**, *8* (5), 690–695. https://doi.org/10.1002/cphc.200600637.

(45) Anderson, J. L.; Ding, R.; Ellern, A.; Armstrong, D. W. Structure and Properties of High Stability Geminal Dicationic Ionic Liquids. *J. Am. Chem. Soc.* **2005**, *127* (2), 593–604. https://doi.org/10.1021/ja046521u.

(46) Montalbán, M. G.; Víllora, G.; Licence, P. Synthesis and Characterization Data of Monocationic and Dicationic Ionic Liquids or Molten Salts. *Data Br.* **2018**, *19*, 769–788. https://doi.org/10.1016/j.dib.2018.05.080.

(47) Sun, Y. X.; Wang, Y. Y.; Shen, B. B.; Zhang, B. X.; Hu, X. M. Synthesis and Investigation of Physico-Chemical Properties of Dicationic Ionic Liquids. *R. Soc. Open Sci.* **2018**, *5* (12). https://doi.org/10.1098/rsos.181230.

(48) Gómez, E.; Calvar, N.; Domínguez, Á. Thermal Behaviour of Pure Ionic Liquids. **2015**. https://doi.org/10.5772/59271.

(49) D'Anna, F.; Nimal Gunaratne, H. Q.; Lazzara, G.; Noto, R.; Rizzo, C.; Seddon, K. R.

Solution and Thermal Behaviour of Novel Dicationic Imidazolium Ionic Liquids. *Org. Biomol. Chem.* **2013**, *11* (35), 5836–5846. https://doi.org/10.1039/c3ob40807h.

(50) Beloqui, A. Supramolecular Assembly of Benzimidazole Derivatives and Applications. In *Chemistry and Applications of Benzimidazole and its Derivatives*; IntechOpen, 2019. https://doi.org/10.5772/intechopen.85333.

(51) Ngo, H. L.; LeCompte, K.; Hargens, L.; McEwen, A. B. Thermal Properties of Imidazolium Ionic Liquids. *Thermochim. Acta* **2000**, *357–358*, 97–102. https://doi.org/10.1016/S0040-6031(00)00373-7.

(52) Huang, W. G.; Zhang, S. M.; Dai, L. Y.; Shan, Y. K. Novel Ionic Liquids Based on the Benzimidazolium Cation. *J. Chem. Res.* **2004**, *2004* (7), 506–507. https://doi.org/10.3184/0308234042037202.

(53) Pike, S. J.; Hutchinson, J. J.; Hunter, C. A. H-Bond Acceptor Parameters for Anions. *J. Am. Chem. Soc.* **2017**, *139* (19), 6700–6706. https://doi.org/10.1021/jacs.7b02008.

(54) Han, H. Y.; Geng, X.; Zhang, B. X.; Meng, J.; Liu, X.; He, X. M.; Liu, Z. G.; Gao, Y. F.; Liu, D.; Hu, X. M. Synthesis of Novel Functional Ionic Liquids and Their Application in Biomass. *RSC Adv.* **2019**, *9* (51), 29652–29658. https://doi.org/10.1039/c9ra06243b.

(55) Zhang, Q.; Li, Z.; Zhang, J.; Zhang, S.; Zhu, L.; Yang, J.; Zhang, X.; Deng, Y. Physicochemical Properties of Nitrile-Functionalized Ionic Liquids. *J. Phys. Chem. B* **2007**, *111* (11), 2864–2872. https://doi.org/10.1021/jp067327s.

(56) Clarke, C. J.; Puttick, S.; Sanderson, T. J.; Taylor, A. W.; Bourne, R. A.; Lovelock, K. R. J.; Licence, P. Thermal Stability of Dialkylimidazolium Tetrafluoroborate and

Hexafluorophosphate Ionic Liquids:: Ex Situ Bulk Heating to Complement in Situ Mass Spectrometry. *Phys. Chem. Chem. Phys.* **2018**, *20* (24), 16786–16800. https://doi.org/10.1039/c8cp01090k.

(57) Han, X.; Armstrong, D. W. Using Geminal Dicationic Ionic Liquids as Solvents for High-Temperature Organic Reactions. *Org. Lett.* **2005**, *7* (19), 4205–4208. https://doi.org/10.1021/ol051637w.

(58) Clarke, C. J.; Maxwell-Hogg, S.; Smith, E. F.; Hawker, R. R.; Harper, J. B.; Licence, P. Resolving X-Ray Photoelectron Spectra of Ionic Liquids with Difference Spectroscopy. *Phys. Chem. Chem. Phys.* **2019**, *21* (1), 114–123. https://doi.org/10.1039/c8cp06701e.

(59) Lovelock, K. R. J.; Kolbeck, C.; Cremer, T.; Paape, N.; Wasserscheid, P.; Maier, F.; Steinru, H. Influence of Different Substituents on the Surface Composition of Ionic Liquids Studied Using ARXPS Influence of Different Substituents on the Surface Composition of Ionic Liquids Studied. **2009**, 2854–2864. https://doi.org/10.1021/jp810637d.